

Optimal Multi-Objective Wave-Momentum Shaping in Scattering Media

Tristan Nerson,^{1,*} Jakob Hüpf,² Clément Ferise,¹ David Globosits,²
Marlene Hudler,² Matthieu Malléjac,^{3,4} Stefan Rotter,² and Romain Fleury^{1,†}

¹*Laboratory of Wave Engineering, School of Electrical Engineering, EPFL, Lausanne, Switzerland*

²*Institute for Theoretical Physics, Vienna University of Technology (TU Wien), A-1040 Vienna, Austria*

³*Univ. Bordeaux, CNRS, Bordeaux INP, I2M, UMR 5295, F-33400, Talence, France*

⁴*Arts et Metiers Institute of Technology, CNRS,
Bordeaux INP, I2M, UMR 5295, F-33400 Talence, France*

(Dated: December 1, 2025)

Radiation forces and torques are key to manipulating objects with acoustic or electromagnetic waves. An important concept in this context is the Generalized Wigner–Smith (GWS) matrix, which has previously been primarily studied for optimizing radiation forces and torques on single objects embedded inside complex scattering environments. Here, we develop a unified scattering framework that rigorously establishes this connection for arbitrary inhomogeneous, lossless electromagnetic and acoustic media, as well as for controlling multiple objects individually. Variational identities relate parametric changes of the medium to perturbations of the scattering fields, from which the GWS matrix emerges as a natural generator of radiation forces and torques. For a single object, its extremal eigenstates yield maximal force or torque along a chosen direction; for multiple objects, the same framework defines Pareto-optimal compromises among competing objectives and reveals uncertainty relations for their simultaneous optimization. This establishes a comprehensive foundation towards collective and selective manipulation of objects in complex media.

When propagating through complex media, waves – acoustic or electromagnetic, among others – undergo repeated scattering events due to inhomogeneities, which challenges our ability to control and predict their propagation. Foundational works in acoustics by Fink and colleagues showed that wavefronts can be time-reversed to refocus through complex media, revealing that multiple scattering does not necessarily lead to information loss [1, 2]. Building on these ideas, Vellekoop et al. later demonstrated that tailored wavefronts can focus light through opaque, strongly scattering media, marking the experimental inception of the field of wavefront shaping in optics [3, 4], and further accelerated by the experimental measurement of the optical transmission matrix (a subset of the full scattering matrix \mathbf{S} capturing the far-field information of the wave propagation) [5]. A key concept in modern wavefront shaping is the use of the Generalized Wigner-Smith (GWS) matrix, defined as

$$\mathbf{Q}_\alpha = j\mathbf{S}^\dagger \partial_\alpha \mathbf{S}, \quad (1)$$

where α denotes a given global or local parameter of the scattering region, and \dagger denotes the conjugate transpose. Here, we assume the $+j\omega t$ time-harmonic convention, with the angular frequency ω . First described in nuclear and mesoscopic quantum physics [6–8], this matrix was repurposed as a practical tool to optimize incoming waves for given operations [9, 10]. This has notably found applications in wave focusing, particle cooling and trapping, information retrieval, inverse design and analysis of scattering resonances [11–21].

Beyond controlling the spatial distribution of wave amplitude or phase, many applications rely on the mechanical action that waves exert on objects through radiation

forces and torques. A connection between these mechanical effects and the GWS matrix has previously been identified, showing that its extremal states can maximize the response of a single object undergoing a small translation or rotation in a scattering environment [9, 10, 22, 23]. What has been lacking, however, is a general theoretical framework that unifies these ideas for arbitrary acoustic or electromagnetic media and extends them to the individual control of multiple objects.

Here, we develop such a framework based on variational relations that link parametric changes of the medium to modifications of the scattering fields, leading naturally to GWS matrices that encode individual forces and torques on multiple particles at once. This multi-objective formulation establishes that compromises between competing mechanical targets are inevitable, with GWS eigenstates defining Pareto-optimal solutions that outperform naive Monte Carlo approaches. In particular, we demonstrate how tailored input states can realize coordinated motion of several objects (Fig. 1a) and establish a fundamental bound governing simultaneous optimization of incompatible objectives. Finally, we identify constrained variants that enable selective manipulation, such as maximizing the force on a target object along a prescribed direction while suppressing its motion in an orthogonal direction and simultaneously constraining forces experienced by some other objects (Fig. 1b).

Radiation forces in inhomogeneous media— In the following, we assume lossless propagation, under which the \mathbf{S} -matrix is unitary. In acoustics, we are interested in the radiation force density in a fluid containing some inclusions. It is assumed that the inclusions, even though potentially of solid nature, can be modeled as equiva-

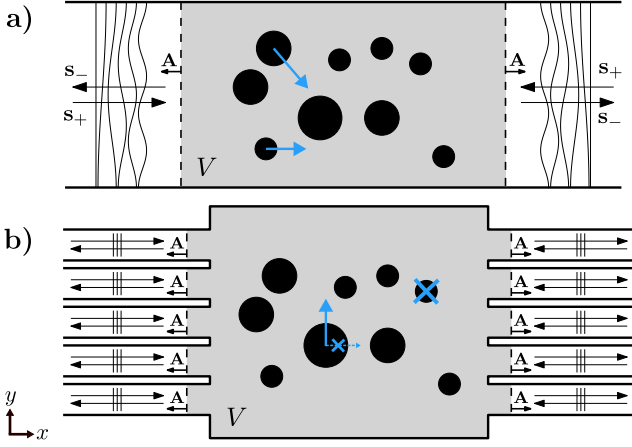


FIG. 1. Two examples of 2D inhomogeneous media described by the scattering matrix formalism, together with two optimization goals. The volume V is represented in gray, comprising both the background and the inclusions, and is delimited by the dashed boundary \mathbf{A} oriented away from the scattering region. **a)** Multimode disordered waveguide in which two objects must be displaced. **b)** Multiport open disordered cavity with monomode waveguides (here plane waves as in acoustics) in which one object must be displaced in the y -direction only, and one object must not be displaced at all.

lent inviscid fluids in which the Euler equations hold, so that the whole medium is described as an inhomogeneous fluid, while any transverse wave is neglected. A rule of thumb is to consider solid inclusions of characteristic size d in which $\omega \ll \pi c_s/d$, where c_s is the shear speed of sound. It has been shown that the time-averaged acoustic body force density can then be written as [24]

$$\bar{\mathbf{f}}_{\text{ac}} = -\frac{1}{4} \left(|p_1|^2 \nabla \kappa_0 + |\mathbf{v}_1|^2 \nabla \rho_0 \right), \quad (2)$$

where κ_0 , ρ_0 , p_1 and \mathbf{v}_1 are the compressibility, density, first order complex pressure and acoustic velocity fields, respectively, with

$$\nabla \cdot \mathbf{v}_1 = -j\omega \kappa_0 p_1 \text{ and } \nabla p_1 = -j\omega \rho_0 \mathbf{v}_1. \quad (3)$$

In electromagnetism, for a linear, isotropic, non-dispersive and lossless inhomogeneous medium with no free charges or currents, the time-averaged force density for harmonic fields is analogous to the one in acoustics [25]:

$$\bar{\mathbf{f}}_{\text{em}} = -\frac{1}{4} \left(|\mathbf{E}|^2 \nabla \varepsilon + |\mathbf{H}|^2 \nabla \mu \right), \quad (4)$$

where ε and μ are the permittivity and permeability of the inhomogeneous medium, respectively, and \mathbf{E} and \mathbf{H} the complex electric and magnetic vector fields. By exploiting the analogy between Eqs. (2) and (4), and using an immittance scattering formalism, we now formulate a general theory of radiation forces expressed as scattering variational integrals.

Impedance formalism of scattering— Following circuit theory nomenclature [26, 27], we introduce effective scattering quantities – hereafter called immittance voltage u_m and current i_m – at a scattering port m as:

$$u_m = \sqrt{2}(s_m^+ + s_m^-), \quad i_m = \sqrt{2}(s_m^+ - s_m^-), \quad (5)$$

where s_m^\pm is the incident (+) and outgoing (−) complex amplitude of the wave, normalized such that $|s_m^\pm|^2$ is equal to the incident/outgoing power at the corresponding port. The scattering matrix \mathbf{S} is defined as $\mathbf{s}_- = \mathbf{S}\mathbf{s}_+$, hence the immittance vectors read

$$\mathbf{u} = \sqrt{2}(\mathbb{1} + \mathbf{S})\mathbf{s}_+, \quad \mathbf{i} = \sqrt{2}(\mathbb{1} - \mathbf{S})\mathbf{s}_+, \quad (6)$$

where $\mathbb{1}$ denotes the identity matrix. In practice, the N ports correspond to the asymptotic modes that couple the scattering region to its environment. In the multimode disordered waveguide of Fig. 1a, they are the propagating guided modes of the homogeneous leads, while in the open cavity of Fig. 1b they are the ones of the attached monomode waveguides. In both cases, the far-field information about the volume V inside the dashed boundary \mathbf{A} is described by its scattering matrix with respect to these ports. Note that by convention, i_m is positive when flowing into the scattering region. Defining the complex Poynting vector as

$$\mathbf{\Pi} = \begin{cases} \frac{1}{2} p_1 \mathbf{v}_1^* & \text{(in acoustics),} \\ \frac{1}{2} \mathbf{E} \times \mathbf{H}^* & \text{(in electromagnetism),} \end{cases} \quad (7a)$$

$$\quad (7b)$$

it can be shown that in both acoustics and electromagnetism [28],

$$-2 \int_A (\mathbf{\Pi} + \mathbf{\Pi}^*) \cdot d\mathbf{A} = \mathbf{u}^\dagger \mathbf{i} + \mathbf{i}^\dagger \mathbf{u}. \quad (8)$$

Equation (8) holds whenever no reactive wave enters the volume V , i.e., the scattering region is only excited via propagating waves from the outside. Experimentally, this often requires placing sources in the far-field, so that all evanescent waves are sufficiently decayed.

Variational integrals— We extend here an important variational integral relation [29] connecting parametric changes occurring in the scattering region to changes of the immittance voltages and currents in the asymptotic regions. We are interested in the variations of the fields δp_1 and $\delta \mathbf{v}_1$ (resp. $\delta \mathbf{E}$ and $\delta \mathbf{H}$) when a parameter α in the system is slightly varied. Consider a system built from N_p spherical particles of diameter d_i and density $\rho_{0,i}$ in a $\rho_0^{(b)}(\mathbf{r})$ background, such that the density distribution can be written as

$$\rho_0(\mathbf{r}) = \rho_0^{(b)}(\mathbf{r}) + \sum_{i=1}^{N_p} \text{rect}_{d_i}(|\mathbf{r} - \mathbf{r}_i|) \left(\rho_{0,i} - \rho_0^{(b)}(\mathbf{r}) \right), \quad (9)$$

with $\text{rect}_{d_i}(r)$ being the rectangular function of width d_i , and \mathbf{r}_i the positions of the particles. We decide to move the k^{th} particle by $\boldsymbol{\alpha} = \Delta\mathbf{r}$, inducing a local change in the system, and modify the density distribution by changing \mathbf{r}_k into $\mathbf{r}_k + \Delta\mathbf{r}$ in the formula. In a volume V_p surrounding the particle, we assume that the background density is constant and that only the k^{th} term of the sum contributes to the density distribution. We then observe that

$$\nabla\rho_0(\mathbf{r}, \Delta\mathbf{r}) = -\nabla_{\Delta\mathbf{r}}\rho_0(\mathbf{r}, \Delta\mathbf{r}) \quad \text{in } V_p, \quad (10)$$

with $\nabla_{\Delta\mathbf{r}} = (\partial_{\Delta x}, \partial_{\Delta y})$ in 2D. This also applies to the compressibility, the permittivity and the permeability.

Now, we use δ to denote small variations of fields or parameters due to perturbations such that $\delta f = \nabla_{\boldsymbol{\alpha}} f \cdot \delta\boldsymbol{\alpha}$. In acoustics, Eq. (3) leads at first variational order to

$$\nabla \cdot (\delta\mathbf{v}_1) = -j\omega\delta\boldsymbol{\alpha} \cdot \nabla_{\boldsymbol{\alpha}}(\kappa_0 p_1), \quad (11a)$$

$$\nabla(\delta p_1) = -j\omega\delta\boldsymbol{\alpha} \cdot \nabla_{\boldsymbol{\alpha}}(\rho_0 \mathbf{v}_1). \quad (11b)$$

To relate this to the immittance vectors, Eqs. (11a) and (11b) may be combined as follows:

$$-\nabla \cdot (p_1^* \delta\mathbf{v}_1 + \delta p_1 \mathbf{v}_1^*) = j\omega\delta\boldsymbol{\alpha} \cdot \left(|p_1|^2 \nabla_{\boldsymbol{\alpha}} \kappa_0 + |\mathbf{v}_1|^2 \nabla_{\boldsymbol{\alpha}} \rho_0 \right). \quad (12)$$

It is then possible to compute the volume integral of Eq. (12) and use Eq. (8) to obtain

$$\mathbf{u}^\dagger \delta \mathbf{i} + \mathbf{i}^\dagger \delta \mathbf{u} = j\omega\delta\boldsymbol{\alpha} \cdot \int_V \left(|p_1|^2 \nabla_{\boldsymbol{\alpha}} \kappa_0 + |\mathbf{v}_1|^2 \nabla_{\boldsymbol{\alpha}} \rho_0 \right) dV. \quad (13)$$

Derivation details, as well as the electromagnetic equivalent of Eq. (13) are shown in the End Matter. With this, we evidence that the variations of the immittance vectors (at the ports) can be linked to the local changes in the scattering medium.

We now prove the link between these variations, the local radiation force, the GWS matrix and the optimal motion of an object.

Optimal motion of one object — If $\boldsymbol{\alpha}$ is the spatial shift $\Delta\mathbf{r}$, Eq. (10) applies. The volume of integration in Eq. (13) can be reduced from V to V_p since all the $\nabla_{\boldsymbol{\alpha}}$ terms are zero outside of V_p . Using Eqs. (2) and (4) for the time-averaged force densities, the total radiation force $\bar{\mathbf{F}}$ on the volume V_p in the direction of the shift is

$$\bar{\mathbf{F}} \cdot \delta\Delta\mathbf{r} = -\frac{j}{4\omega} (\mathbf{u}^\dagger \delta \mathbf{i} + \mathbf{i}^\dagger \delta \mathbf{u}). \quad (14)$$

Yet, from Eq. (6),

$$\delta\mathbf{u} = \sqrt{2}[(\mathbb{1} + \mathbf{S})\delta\mathbf{s}_+ + \delta(\mathbf{S})\mathbf{s}_+] \quad (15a)$$

$$\delta\mathbf{i} = \sqrt{2}[(\mathbb{1} - \mathbf{S})\delta\mathbf{s}_+ - \delta(\mathbf{S})\mathbf{s}_+] \quad (15b)$$

For a fixed chosen input state, $\delta\mathbf{s}_+ = \mathbf{0}$, and the change in immittance vectors is only due to the parametric change of the \mathbf{S} -matrix:

$$\mathbf{u}^\dagger \delta \mathbf{i} + \mathbf{i}^\dagger \delta \mathbf{u} = -4\mathbf{s}_+^\dagger \mathbf{S}^\dagger \delta(\mathbf{S})\mathbf{s}_+. \quad (16)$$

We extend the GWS matrix defined in Eq. (1) to multi-dimensional parameters $\Delta\mathbf{r}$ to arrive at this normalized GWS matrix:

$$\begin{aligned} \mathbf{Q}_{\Delta\mathbf{r}} &= j\mathbf{S}^\dagger(\hat{\mathbf{e}}_{\mathbf{r}} \cdot \nabla_{\Delta\mathbf{r}})\mathbf{S} \\ &= \frac{1}{|\delta\Delta\mathbf{r}|} (\delta(\Delta x)\mathbf{Q}_{\Delta x} + \delta(\Delta y)\mathbf{Q}_{\Delta y}), \end{aligned} \quad (17)$$

where $\hat{\mathbf{e}}_{\mathbf{r}} = \delta\Delta\mathbf{r}/|\delta\Delta\mathbf{r}|$. The expectation value over the input states is

$$\langle \mathbf{Q}_{\Delta\mathbf{r}} \rangle_{\mathbf{s}_+} = \mathbf{s}_+^\dagger \mathbf{Q}_{\Delta\mathbf{r}} \mathbf{s}_+ = -\frac{j}{4|\delta\Delta\mathbf{r}|} (\mathbf{u}^\dagger \delta \mathbf{i} + \mathbf{i}^\dagger \delta \mathbf{u}). \quad (18)$$

Using Eq. (14), we finally obtain

$$\frac{1}{\omega} \langle \mathbf{Q}_{\Delta\mathbf{r}} \rangle_{\mathbf{s}_+} = \bar{\mathbf{F}} \cdot \hat{\mathbf{e}}_{\mathbf{r}}. \quad (19)$$

Eq. (19) is the central equation of our Letter. Since $\mathbf{Q}_{\Delta\mathbf{r}}$ is Hermitian for a unitary scattering matrix, the projection of the radiation force can be written as a Rayleigh quotient. The Courant–Fischer min–max theorem then ensures that

$$\frac{\lambda_1}{\omega} |\mathbf{s}_+|^2 \leq \bar{\mathbf{F}} \cdot \hat{\mathbf{e}}_{\mathbf{r}} \leq \frac{\lambda_N}{\omega} |\mathbf{s}_+|^2, \quad (20)$$

where the eigenvalues of $\mathbf{Q}_{\Delta\mathbf{r}}$ are ordered as $\lambda_1 \leq \lambda_2 \leq \dots \leq \lambda_N$. Of particular interest are the extremal values of $\bar{\mathbf{F}} \cdot \hat{\mathbf{e}}_{\mathbf{r}}$, which are reached when the incident state coincides with the associated eigenvector, enabling the maximization or minimization of the applied force projection. More generally, if only L out of N ports are accessible, the largest force projection lies between λ_L/ω and λ_N/ω , with typical values in between. In the following, all the expectation values $\langle \cdot \rangle$ are taken with respect to the normalized input state such that $|\mathbf{s}_+|^2 = 1W$.

Optimal motion of multiple objects — When N_d objects are displaced, the variational integrals split into non-overlapping contributions over the disjoint volumes $V_{p,i}$. The total quantity

$$\frac{1}{\omega} \langle \mathbf{Q}_{\Delta\mathbf{r}_{\text{tot}}} \rangle = \frac{1}{|\delta\Delta\mathbf{r}_{\text{tot}}|} \sum_{i=1}^{N_d} |\delta\Delta\mathbf{r}_i| \bar{\mathbf{F}}_i \cdot \hat{\mathbf{e}}_{\mathbf{r}_i}, \quad (21)$$

therefore measures the infinitesimal (virtual) work of the radiation force on the system. Here, $\delta\Delta\mathbf{r}_{\text{tot}} = (\delta\Delta\mathbf{r}_1, \dots, \delta\Delta\mathbf{r}_{N_d})$ is the stacked displacement vector and $\bar{\mathbf{F}}_i \cdot \hat{\mathbf{e}}_{\mathbf{r}_i}$ is the time-averaged force on the i^{th} object in the direction of its push. Without loss of generality, we can focus on the generic case of two objects ($N_d = 2$). Because $\mathbf{Q}_{\Delta\mathbf{r}_1}$ and $\mathbf{Q}_{\Delta\mathbf{r}_2}$ typically do not commute, they cannot, in general, be diagonalized simultaneously; hence, no single incident state maximizes both projections $\bar{\mathbf{F}}_1 \cdot \hat{\mathbf{e}}_{\mathbf{r}_1}$ and $\bar{\mathbf{F}}_2 \cdot \hat{\mathbf{e}}_{\mathbf{r}_2}$ [30]. Yet, the largest eigenvector of $\mathbf{Q}_{\Delta\mathbf{r}_{\text{tot}}}$ maximizes the sum of the projections. Consequently, the multi-object formulation can be

directly interpreted through the lens of multi-objective optimization [31]. Each $\mathbf{F}_i \cdot \hat{\mathbf{e}}_{\mathbf{r}_i}$ defines an objective to be maximized and $\langle \mathbf{Q}_{\Delta \mathbf{r}_{\text{tot}}} \rangle$ corresponds to a so-called linear scalarization of this problem (i.e., forming a weighted sum to be maximized), with the coefficients $|\delta \Delta \mathbf{r}_i|$ playing the role of optimization weights. An extension of the theory to optimal torque on objects is proposed in the End Matter. For two objectives – such as displacing/rotating two objects along/about one direction each – the feasible set of force components corresponds to the joint numerical range of two Hermitian matrices, which is always convex [32]. This is also true for three objectives when $N > 2$ [33]. In these cases, it is known that linear scalarization generates an entire Pareto front [31] – that is, the set of solutions where no objective can be improved without degrading another. We then discover that the GWS explores the full set of such compromises. For four or more objectives, convexity can fail, and the GWS recovers only the exposed subset of the Pareto front, leaving non-convex regions inaccessible.

As an example, a bi-objective Pareto front for the simultaneous translation of two objects in a 20-port disordered acoustic cavity is simulated in Fig. 2a (red solid line). For comparison, we also show the corresponding force projections for 10^7 random inputs represented by the distribution of dots, the color of which indicates the number of occurrences. Strikingly, the Pareto front obtained from the GWS procedure greatly outperforms all the random inputs, thus demonstrating that naive Monte Carlo exploration of the input space cannot realistically be implemented to tailor radiation forces in complex media. In the Supplemental Material, we conjecture that the force projections – whose respective probability distributions are B-splines [34–37] – can never compete with the GWS procedure for sufficiently high number of ports. Moreover, the Pareto front is compared to the result of a heuristic procedure also based on the GWS matrix, where a linear combination of eigenvectors of $\mathbf{Q}_{\Delta \mathbf{r}_1}$ and $\mathbf{Q}_{\Delta \mathbf{r}_2}$ is performed (green dashed line). In terms of maximum force projections, the newly proposed procedure consistently outperforms this technique, hitherto viewed as the benchmark approach and closely aligned with the most recent literature [23]. The result of the Pareto optimization is shown in Fig. 2b, where blue arrows correspond to the objectives, and black arrows correspond to the net forces exerted on the objects, computed via the Brillouin stress tensor. Further examples can be found in the Supplemental Material.

Uncertainty relation— In two-objective optimization with GWS matrices, one seeks to simultaneously maximize the expectation values of the matrices \mathbf{Q}_α and \mathbf{Q}_β , corresponding for instance to distinct forces or torques on one or multiple objects. We define the deficits from utopia values (highest eigenvalues) for a given input state

\mathbf{s}_+ as

$$\epsilon_\alpha = \lambda_N(\mathbf{Q}_\alpha) - \langle \mathbf{Q}_\alpha \rangle, \quad \epsilon_\beta = \lambda_N(\mathbf{Q}_\beta) - \langle \mathbf{Q}_\beta \rangle. \quad (22)$$

A direct application of the Schrödinger-Robertson uncertainty relation [38], combined with the Bhatia-Davis inequality [39], yields the following bound:

$$\epsilon_\alpha \epsilon_\beta \geq \frac{\frac{1}{4} |\langle [\mathbf{Q}_\alpha, \mathbf{Q}_\beta] \rangle|^2 + \text{Cov}(\mathbf{Q}_\alpha, \mathbf{Q}_\beta)^2}{(\langle \mathbf{Q}_\alpha \rangle - \lambda_1(\mathbf{Q}_\alpha))(\langle \mathbf{Q}_\beta \rangle - \lambda_1(\mathbf{Q}_\beta))}. \quad (23)$$

Here, the symmetrized covariance is

$$\text{Cov}(\mathbf{Q}_\alpha, \mathbf{Q}_\beta) = \frac{1}{2} \langle \{ \mathbf{Q}_\alpha - \langle \mathbf{Q}_\alpha \rangle, \mathbf{Q}_\beta - \langle \mathbf{Q}_\beta \rangle \} \rangle, \quad (24)$$

and $[\mathbf{A}, \mathbf{B}]$ and $\{\mathbf{A}, \mathbf{B}\}$ denote the commutator and anti-commutator, respectively. The right-hand side of Eq. (23) cannot vanish unless the expectation value of the commutator vanishes and the two GWS matrices are uncorrelated in the chosen input state. In particular, the case $\epsilon_\alpha = \epsilon_\beta = 0$ corresponds to the situation where the two matrices share the same eigenstate associated with their respective maximal eigenvalues, which is very non-generic. This inequality highlights that the two objectives cannot be simultaneously optimized: reducing the deficit for one inevitably increases the other, which is precisely the trade-off structure captured by the Pareto front.

Constrained optimization— Another interesting problem is the one of maximizing the expectation value of a given \mathbf{Q}_α while enforcing N_c constraints on the expectation value of other objectives \mathbf{Q}_{β_i} :

$$\begin{aligned} \max_{\mathbf{s}_+ \in \mathbb{C}^N} \quad & \langle \mathbf{Q}_\alpha \rangle \\ \text{s.t.} \quad & \langle \mathbf{Q}_{\beta_i} \rangle \triangleright_i b_i, \quad i = 1, \dots, N_c \\ & \mathbf{s}_+^\dagger \mathbf{s}_+ = 1, \end{aligned} \quad (25)$$

where “ \triangleright ” can signify “=”, “ \leq ” or “ \geq ”. This is known as a complex-valued homogeneous quadratically constrained quadratic program, and is generally an NP-hard problem for $N_c > 2$ [40, 41]. However, local optima are generally easy to find, enabling the selective manipulation of objects.

As an example, we show in Fig. 2c the manipulation of object ① in the y -direction only, while object ② is kept still, i.e., $\langle \mathbf{Q}_{\Delta y_1} \rangle$ is maximized, while $\langle \mathbf{Q}_{\Delta x_1} \rangle$, $\langle \mathbf{Q}_{\Delta x_2} \rangle$ and $\langle \mathbf{Q}_{\Delta y_2} \rangle$ are forced to be close to zero (a 10^8 magnitude difference is observed in our simulation between $\langle \mathbf{Q}_{\Delta y_1} \rangle$ and other expectation values). The Gurobi Optimization solver is used for this task [42]. It can be readily seen that the resulting wave field indeed manages to compensate local forces (represented by the red arrows in the inset of Fig. 2c) on the objects and cancel the desired force projections.

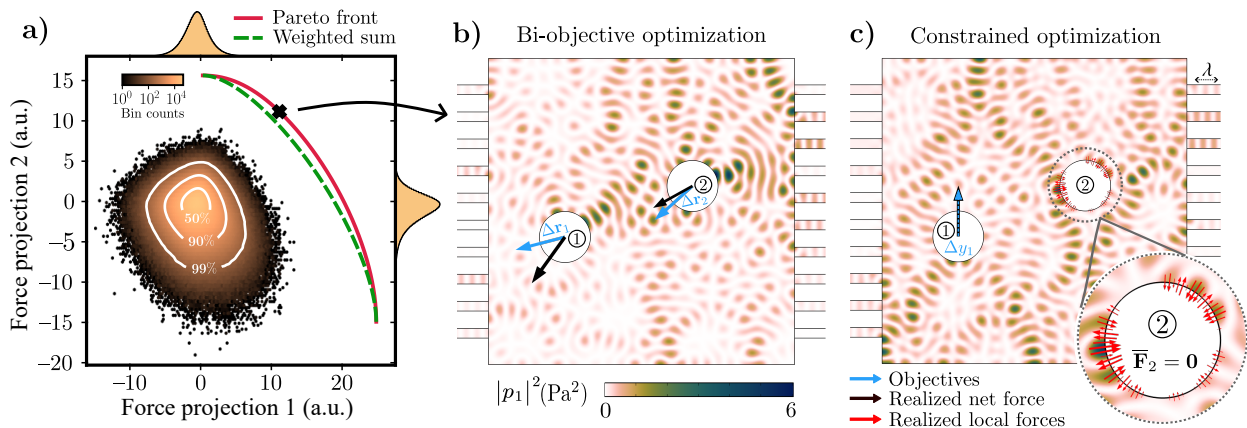


FIG. 2. Collective and selective manipulation of objects in scattering media. **a)** Bi-objective optimization: probability distribution of the force projections on two objects for 10^7 random input states. The marginal distributions form B-splines. The Pareto front (red solid line) is compared to a heuristic weighted sum of eigenstates (green dashed line). **b)** Full wave simulation of the squared acoustic pressure field corresponding to the Pareto-optimal solution for which the force projections are equal, i.e., $\langle \mathbf{Q}_{\Delta \mathbf{r}_1} \rangle = \langle \mathbf{Q}_{\Delta \mathbf{r}_2} \rangle$. The blue arrows are the objectives and the black arrows are the net forces exerted on the objects. **c)** Constrained optimization: the object ① is displaced along the vertical direction only (net force in black perfectly overlapping with the objective in blue), while the object ② experiences local forces (small red arrows with their width and length logarithmically scaling with the local force magnitude) which globally compensate to obtain zero net force. The wavelength λ is shown on the right.

Discussion— We have shown that radiation forces in complex media can be optimized through the Generalized Wigner–Smith matrix: its extremal eigenstates maximize force or torque projections on a single object, while in the multi-object case they realize Pareto-optimal trade-offs among competing objectives. Together with a realistic demonstration of constrained optimization of objects’ motion along targeted directions, our Letter establishes a unified framework across acoustics and electromagnetism, and provides a principled route to coordinated manipulation in strongly scattering environments. In addition, the uncertainty relation of Eq. (23) quantifies the fundamental trade-offs that emerge when simultaneously optimizing forces or torque components. From the present study, the state-of-the-art strategies of Horodynski et al. [10] (superposition of two torque eigenstates to suppress unwanted linear forces) and Orazbayev et al. [23] (separate optimization of $\mathbf{Q}_{\Delta x}$ and $\mathbf{Q}_{\Delta y}$ instead of diagonalizing $\mathbf{Q}_{\Delta \mathbf{r}}$) can be seen as important first steps, but they may fail or become suboptimal in a general situation; the present framework unifies and extends these ideas, providing a systematic route to the truly optimal radiation force control.

Beyond fundamental interest, our results may contribute to the development of in-vivo precision therapy and drug delivery, where navigation through deep tissues requires controlling radiation forces in multiply scattering media [43–49]. We also note interesting connections between our findings and a recent preprint [50], which investigates the simultaneous control of transmission, reflection and absorption. Our Letter strongly suggests

that the notion of Pareto-optimality for multi-objective wavefront shaping introduced here could offer a general framework that naturally extends from optimal radiation forces and torques to other joint-control scenarios such as those considered in Ref. [50].

Acknowledgments— This work was supported by the Swiss National Science Foundation (SNSF) under the grant No. 10001567.

* tristan.nerson@epfl.ch

† romain.fleury@epfl.ch

- [1] M. Fink, D. Cassereau, A. Derode, C. Prada, P. Roux, M. Tanter, J.-L. Thomas, and F. Wu, Time-reversed acoustics, *Rep. Prog. Phys.* **63**, 1933 (2000).
- [2] M. Horodynski, D. Bouchet, M. Kühmayer, and S. Rotter, Invariance property of the Fisher information in scattering media, *Phys. Rev. Lett.* **127**, 233201 (2021).
- [3] I. M. Vellekoop and A. P. Mosk, Focusing coherent light through opaque strongly scattering media, *Opt. Lett.* **32**, 2309 (2007).
- [4] A. P. Mosk, A. Lagendijk, G. Leroosey, and M. Fink, Controlling waves in space and time for imaging and focusing in complex media, *Nat. Photon.* **6**, 283 (2012).
- [5] S. M. Popoff, G. Leroosey, R. Carminati, M. Fink, A. C. Boccara, and S. Gigan, Measuring the transmission matrix in optics: an approach to the study and control of light propagation in disordered media, *Phys. Rev. Lett.* **104**, 100601 (2010).
- [6] F. T. Smith, Lifetime matrix in collision theory, *Phys. Rev.* **118**, 349 (1960).

- [7] M. Froissart, M. L. Goldberger, and K. M. Watson, Spatial separation of events in S -matrix theory, *Phys. Rev.* **131**, 2820 (1963).
- [8] P. W. Brouwer, K. M. Frahm, and C. W. J. Beenakker, Quantum mechanical time-delay matrix in chaotic scattering, *Phys. Rev. Lett.* **78**, 4737 (1997).
- [9] P. Ambichl, A. Brandstötter, J. Böhm, M. Kühmayer, U. Kuhl, and S. Rotter, Focusing inside disordered media with the generalized Wigner-Smith operator, *Phys. Rev. Lett.* **119**, 033903 (2017).
- [10] M. Horodyski, M. Kühmayer, A. Brandstötter, K. Pichler, Y. V. Fyodorov, U. Kuhl, and S. Rotter, Optimal wave fields for micromanipulation in complex scattering environments, *Nat. Photon.* **14**, 149 (2020).
- [11] D. Bouchet, S. Rotter, and A. P. Mosk, Maximum information states for coherent scattering measurements, *Nat. Phys.* **17**, 564 (2021).
- [12] M. W. Matthès, Y. Bromberg, J. de Rosny, and S. M. Popoff, Learning and avoiding disorder in multimode fibers, *Phys. Rev. X* **11**, 021060 (2021).
- [13] P. del Hougne, K. B. Yeo, P. Besnier, and M. Davy, Coherent wave control in complex media with arbitrary wavefronts, *Phys. Rev. Lett.* **126**, 193903 (2021).
- [14] M. Horodyski, M. Kühmayer, C. Ferise, S. Rotter, and M. Davy, Anti-reflection structure for perfect transmission through complex media, *Nature* **607**, 281 (2022).
- [15] J. Hüpf, N. Bachelard, M. Kaczvinski, M. Horodyski, M. Kühmayer, and S. Rotter, Optimal cooling of multiple levitated particles through far-field wavefront shaping, *Phys. Rev. Lett.* **130**, 083203 (2023).
- [16] J. Sol, L. Le Magoarou, and P. del Hougne, Optimal blind focusing on perturbation-inducing targets in sub-unitary complex media, *Laser Photonics Rev.* **19**, 2400619 (2024).
- [17] U. G. Bütaitė, C. Sharp, M. Horodyski, G. M. Gibson, M. J. Padgett, S. Rotter, J. M. Taylor, and D. B. Phillips, Photon-efficient optical tweezers via wavefront shaping, *Sci. Adv.* **10**, eadi7792 (2024).
- [18] D. Globosits, J. Hüpf, and S. Rotter, Pseudounitary Floquet scattering matrix for wave-front shaping in time-periodic photonic media, *Phys. Rev. A* **110**, 053515 (2024).
- [19] A. Goicoechea, J. Hüpf, S. Rotter, F. Sarrazin, and M. Davy, Detecting and focusing on a nonlinear target in a complex medium, *Phys. Rev. Lett.* **134**, 183802 (2025).
- [20] N. Byrnes and M. R. Foreman, Perturbing scattering resonances in non-hermitian systems: a generalized Wigner-Smith operator formulation, *Newton* **1**, 100194 (2025).
- [21] K. Y. Bliokh, Z. Kuang, and S. Rotter, Dynamic and geometric shifts in wave scattering, *Rep. Prog. Phys.* **88**, 107901 (2025).
- [22] M. Horodyski, T. Reiter, M. Kühmayer, and S. Rotter, Tractor beams with optimal pulling force using structured waves, *Phys. Rev. A* **108**, 023504 (2023).
- [23] B. Orazbayev, M. Malléjac, N. Bachelard, S. Rotter, and R. Fleury, Wave-momentum shaping for moving objects in heterogeneous and dynamic media, *Nat. Phys.* **20**, 1441 (2024).
- [24] J. T. Karlsen, P. Augustsson, and H. Bruus, Acoustic force density acting on inhomogeneous fluids in acoustic fields, *Phys. Rev. Lett.* **117**, 114504 (2016).
- [25] B. Anghinoni, G. Flizikowski, L. Malacarne, M. Partanen, S. Bialkowski, and N. Astrath, On the formulations of the electromagnetic stress-energy tensor, *Ann. Phys.* **443**, 169004 (2022).
- [26] A. Zemanian, An n -port realizability theory based on the theory of distributions, *IEEE Trans. Circuit Theory* **10**, 265 (1963).
- [27] R. H. Dicke, General microwave circuit theorems, in *Principles of Microwave Circuits*, IET Electromagnetic Waves Series No. 25, edited by C. G. Montgomery, R. H. Dicke, and E. M. Purcell (IET, 1987) pp. 130–161.
- [28] A. A. Barybin, Modal expansions and orthogonal complements in the theory of complex media waveguide excitation by external sources for isotropic, anisotropic, and bianisotropic media, *Prog. Electromagn. Res.* **19**, 241 (1998).
- [29] J. Hüpf, N. Bachelard, M. Kaczvinski, M. Horodyski, M. Kühmayer, and S. Rotter, Optimal cooling of multiple levitated particles: Theory of far-field wavefront shaping, *Phys. Rev. A* **107**, 023112 (2023).
- [30] An exception occurs if the two matrices happen to share the same eigenvector associated with their maximal eigenvalues. This non-generic case is understood in Eq. (23) by observing that what matters is not ultimately the commutation of the two matrices but the vanishing of the expectation value of the commutator.
- [31] K. Miettinen, *Nonlinear multiobjective optimization*, edited by F. S. Hillier, International Series in Operations Research & Management Science, Vol. 12 (Springer US, Boston, MA, 1999).
- [32] F. Hausdorff, Der wertvorrat einer bilinearform, *Math. Z.* **3**, 314 (1919).
- [33] M. K. Fan and A. L. Tits, On the generalized numerical range, *Linear Multilinear Algebra* **21**, 313 (1987).
- [34] T. Gallay and D. Serre, Numerical measure of a complex matrix, *Commun. Pure Appl. Math.* **65**, 287 (2012).
- [35] C. F. Dunkl, P. Gawron, J. A. Holbrook, Z. Puchała, and K. Życzkowski, Numerical shadows: measures and densities on the numerical range, *Linear Algebra Its Appl.* **434**, 2042 (2011).
- [36] L. Campos Venuti and P. Zanardi, Probability density of quantum expectation values, *Phys. Lett. A* **377**, 1854 (2013).
- [37] Y. Wang and C. Guo, Probability distribution for coherent transport of random waves (2025), arXiv:2511.04602 [physics.optics].
- [38] E. Schrödinger, About Heisenberg uncertainty relation (1999), arXiv:quant-ph/9903100 [quant-ph].
- [39] R. Bhatia and C. Davis, A better bound on the variance, *Am. Math. Mon.* **107**, 353 (2000).
- [40] Y. Huang and D. P. Palomar, Rank-constrained separable semidefinite programming with applications to optimal beamforming, *IEEE Trans. Signal Process.* **58**, 664 (2010).
- [41] Z.-Q. Luo, W.-K. Ma, A. M.-C. So, Y. Ye, and S. Zhang, Semidefinite relaxation of quadratic optimization problems, *IEEE Signal Process. Mag.* **27**, 20 (2010).
- [42] Gurobi Optimization, LLC, Gurobi Optimizer Reference Manual (2024).
- [43] A. Del Campo Fonseca and D. Ahmed, Ultrasound robotics for precision therapy, *Adv. Drug Deliv. Rev.* **205**, 115164 (2024).
- [44] M. A. Ghanem, A. D. Maxwell, Y.-N. Wang, B. W. Cunitz, V. A. Khokhlova, O. A. Sapozhnikov, and M. R. Bailey, Noninvasive acoustic manipulation of objects in a living body, *Proc. Natl. Acad. Sci. U.S.A.* **117**, 16848 (2020).

- [45] W.-C. Lo, C.-H. Fan, Y.-J. Ho, C.-W. Lin, and C.-K. Yeh, Tornado-inspired acoustic vortex tweezer for trapping and manipulating microbubbles, *Proc. Natl. Acad. Sci. U.S.A.* **118**, e2023188118 (2021).
- [46] A. Del Campo Fonseca, C. Glück, J. Droux, Y. Ferry, C. Frei, S. Wegener, B. Weber, M. El Amki, and D. Ahmed, Ultrasound trapping and navigation of microrobots in the mouse brain vasculature, *Nat. Commun.* **14**, 5889 (2023).
- [47] Y. Yang, Y. Yang, D. Liu, Y. Wang, M. Lu, Q. Zhang, J. Huang, Y. Li, T. Ma, F. Yan, and H. Zheng, In-vivo programmable acoustic manipulation of genetically engineered bacteria, *Nat. Commun.* **14**, 3297 (2023).
- [48] M. Medany, L. Piglia, L. Achenbach, S. K. Mukkavilli, and D. Ahmed, Model-based reinforcement learning for ultrasound-driven autonomous microrobots, *Nat. Mach. Intell.* **7**, 1076 (2025).
- [49] R. Burstow and A. N. Pouliopoulos, Evaluating the accuracy of acoustic holograms for precise spatial targeting within the brain, *npj Acoust.* **1**, 24 (2025).
- [50] S. Li, D. Kim, S. Fan, and C. Guo, Joint control of coherent transmission, reflection, and absorption (2025), arXiv:2511.04788 [physics.optics].
- [51] P. Blanchard and E. Brüning, Inner product spaces and Hilbert spaces, in *Mathematical Methods in Physics*, Progress in Mathematical Physics, Vol. 69 (Birkhäuser, Cham, 2015) pp. 213–225.
- [52] I. Toftul, S. Golat, F. J. Rodríguez-Fortuño, F. Nori, Y. Kivshar, and K. Y. Bliokh, Radiation forces and torques in optics and acoustics (2025), arXiv:2410.23670 [physics.optics].
- [53] P. L. Marston and J. H. Crichton, Radiation torque on a sphere caused by a circularly-polarized electromagnetic wave, *Phys. Rev. A* **30**, 2508 (1984).
- [54] L. Zhang and P. L. Marston, Angular momentum flux of nonparaxial acoustic vortex beams and torques on axisymmetric objects, *Phys. Rev. E* **84**, 065601 (2011).
- [55] G. T. Silva, T. P. Lobo, and F. G. Mitri, Radiation torque produced by an arbitrary acoustic wave, *EPL* **97**, 54003 (2012).
- [56] M. Smagin, I. Toftul, K. Y. Bliokh, and M. Petrov, Acoustic lateral recoil force and stable lift of anisotropic particles, *Phys. Rev. Appl.* **22**, 064041 (2024).
- [57] P. C. Chaumet and A. Rahmani, Electromagnetic force and torque on magnetic and negative-index scatterers, *Opt. Express* **17**, 2224 (2009).
- [58] Y. E. Lee, K. H. Fung, D. Jin, and N. X. Fang, Optical torque from enhanced scattering by multipolar plasmonic resonance, *Nanophotonics* **3**, 343 (2014).
- [59] M. Nieto-Vesperinas, Optical torque on small bi-isotropic particles, *Opt. Lett.* **40**, 3021 (2015).

End Matter

Derivation details and electromagnetic equivalent of Eq. (13)— For a given physical state a , Eq. (8) reads in acoustics

$$P(a) \equiv - \int_A (p_{1a} \mathbf{v}_{1a}^* + p_{1a}^* \mathbf{v}_{1a}) \cdot d\mathbf{A} = \mathbf{u}_a^\dagger \mathbf{i}_a + \mathbf{i}_a^\dagger \mathbf{u}_a. \quad (26)$$

$$\frac{P(a+b) + jP(a+jb) - [P(a-b) + jP(a-jb)]}{4} = - \int_A (p_{1a} \mathbf{v}_{1b}^* + p_{1b}^* \mathbf{v}_{1a}) \cdot d\mathbf{A} = \mathbf{u}_b^\dagger \mathbf{i}_a + \mathbf{i}_b^\dagger \mathbf{u}_a. \quad (27)$$

Taking the complex conjugate of Eq. (27) for the states $a \rightarrow (p_1, \mathbf{v}_1, \mathbf{u}, \mathbf{i})$ and $b \rightarrow (\delta p_1, \delta \mathbf{v}_1, \delta \mathbf{u}, \delta \mathbf{i})$, we obtain

$$- \int_A (p_1^* \delta \mathbf{v}_1 + \delta p_1 \mathbf{v}_1^*) \cdot d\mathbf{A} = \mathbf{u}^\dagger \delta \mathbf{i} + \mathbf{i}^\dagger \delta \mathbf{u}. \quad (28)$$

Applying the divergence theorem to the volume integral of Eq. (12) and combining with Eq. (28) directly leads to Eq. (13).

In electromagnetism, Maxwell-Faraday and -Ampère laws in frequency domain give

$$\nabla \times \delta \mathbf{E} = -j\omega \delta \boldsymbol{\alpha} \cdot \nabla_{\boldsymbol{\alpha}} (\mu \mathbf{H}) \quad (29a)$$

$$\nabla \times \delta \mathbf{H} = j\omega \delta \boldsymbol{\alpha} \cdot \nabla_{\boldsymbol{\alpha}} (\varepsilon \mathbf{E}) \quad (29b)$$

and

$$\begin{aligned} -\nabla \cdot (\mathbf{E}^* \times \delta \mathbf{H} + \delta \mathbf{E} \times \mathbf{H}^*) \\ = j\omega \delta \boldsymbol{\alpha} \cdot (|\mathbf{E}|^2 \nabla_{\boldsymbol{\alpha}} \varepsilon + |\mathbf{H}|^2 \nabla_{\boldsymbol{\alpha}} \mu), \end{aligned} \quad (30)$$

By extension, it is possible to compose any other physical state $a \pm b$ or $a \pm jb$. Using the linearity of p_1 , \mathbf{v}_1 , \mathbf{u} and \mathbf{i} , one can verify the so-called polarization identity [51]:

from which Eq. (30) gives

$$\mathbf{u}^\dagger \delta \mathbf{i} + \mathbf{i}^\dagger \delta \mathbf{u} = j\omega \delta \boldsymbol{\alpha} \cdot \int_V (|\mathbf{E}|^2 \nabla_{\boldsymbol{\alpha}} \varepsilon + |\mathbf{H}|^2 \nabla_{\boldsymbol{\alpha}} \mu) dV. \quad (31)$$

This is completely analogous to the acoustic case and yields the same end result.

Optimal torque— Rotations enter the variational identities Eqs. (13) and (31) through the generator of infinitesimal rigid rotations: a small angle $\delta \boldsymbol{\theta}$ about a pivot point \mathbf{r}_0 moves each material point by $\delta \mathbf{r} = \delta \boldsymbol{\theta} \times (\mathbf{r} - \mathbf{r}_0)$. This gives the parametric derivative $\nabla_{\boldsymbol{\theta}} = -(\mathbf{r} - \mathbf{r}_0) \times \nabla$. Defining the time-averaged torque $\bar{\boldsymbol{\tau}}(\mathbf{r}_0)$ as

$$\bar{\boldsymbol{\tau}}(\mathbf{r}_0) = \int_V (\mathbf{r} - \mathbf{r}_0) \times \bar{\mathbf{f}} dV, \quad (32)$$

one obtains

$$\bar{\boldsymbol{\tau}}(\mathbf{r}_0) \cdot \delta \Delta \boldsymbol{\theta} = -\frac{j}{4\omega} \left(\mathbf{u}^\dagger \delta \mathbf{i} + \mathbf{i}^\dagger \delta \mathbf{u} \right). \quad (33)$$

Then, in analogy with the linear force case, the GWS reads

$$\frac{1}{\omega} \langle \mathbf{Q}_\theta \rangle = \bar{\boldsymbol{\tau}}(\mathbf{r}_0) \cdot \hat{\mathbf{n}}, \quad (34)$$

and

$$\frac{1}{\omega} \langle \mathbf{Q}_{\boldsymbol{\theta}_{\text{tot}}}^{(\mathbf{r}_{0,i})} \rangle = \frac{1}{|\delta \boldsymbol{\theta}_{\text{tot}}|} \sum_{i=1}^{N_d} |\delta \boldsymbol{\theta}_i| \bar{\boldsymbol{\tau}}_i(\mathbf{r}_{0,i}) \cdot \hat{\mathbf{n}}_i, \quad (35)$$

where $\hat{\mathbf{n}} = \delta \boldsymbol{\theta} / |\delta \boldsymbol{\theta}|$. Interestingly, for axisymmetric objects around $\boldsymbol{\theta}$ (such as the discs in Fig. 2), $\mathbf{Q}_\theta = \mathbf{0}$, and no input state can transfer angular momentum to the objects. This counter-intuitive result, holding in general for any lossless scattering, was already discovered in both acoustics and electromagnetism via other methods, see for example Refs. [52–59].

SUPPLEMENTAL MATERIAL

Statistics of expectation values

The probability density of expectation values of any Hermitian matrix \mathbf{Q}_α over some random input states forms a unimodal non-negative B-spline (also called an M-spline) of degree $N - 2$, with knots corresponding to the eigenvalues of the matrix:

$$f_{\langle \mathbf{Q}_\alpha \rangle}(\xi) = (N - 1) \sum_{i=1}^N \frac{\max(0, \lambda_i - \xi)^{N-2}}{\prod_{j \neq i} (\lambda_i - \lambda_j)}. \quad (36)$$

Examples of this distribution for some random Hermitian matrices are given in Fig. 3.

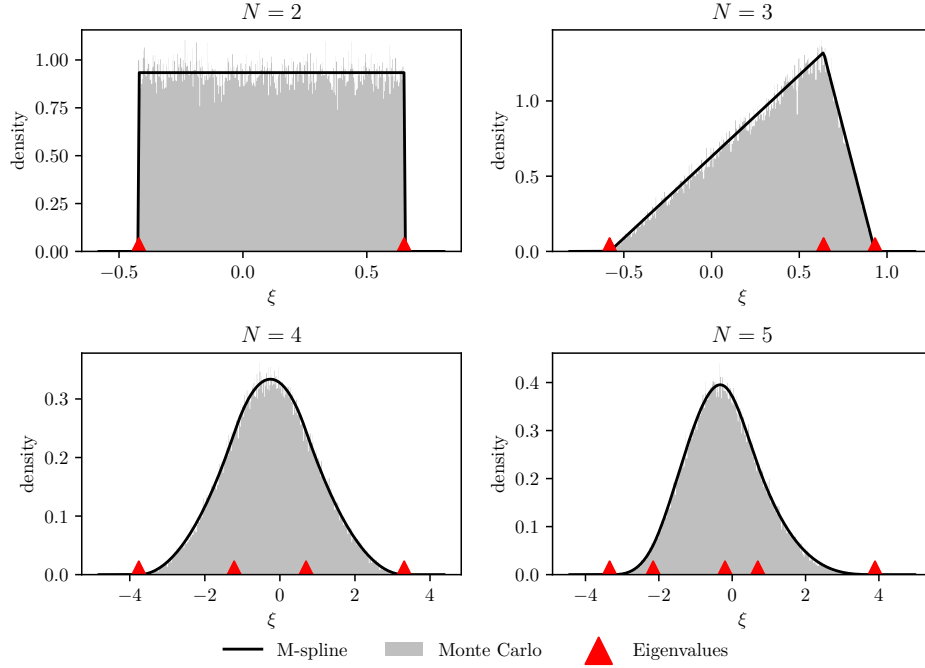


FIG. 3. Probability density function of expectation values of Hermitian matrices of size N . Comparison between 10^5 random input states (in grey) and the theoretical M-spline (black curves).

The expected value of $\langle \mathbf{Q}_\alpha \rangle$ is

$$\mathbb{E}(\langle \mathbf{Q}_\alpha \rangle) = \frac{\text{tr}(\mathbf{Q}_\alpha)}{N}, \quad (37)$$

and the variance is

$$\text{Var}(\langle \mathbf{Q}_\alpha \rangle) = \frac{\frac{\text{tr}(\mathbf{Q}_\alpha^2)}{N} - \left(\frac{\text{tr}(\mathbf{Q}_\alpha)}{N} \right)^2}{N + 1} \leq \frac{\max(|\lambda_1|, |\lambda_N|)^2}{N + 1}, \quad (38)$$

which goes to zero for large N , since $|\lambda_1|$ and $|\lambda_N|$ are physically bounded. The probability that the expectation value on a random input state approaches the largest eigenvalue of \mathbf{Q}_α up to a small fixed parameter ϵ is

$$\mathbb{P}(\langle \mathbf{Q}_\alpha \rangle > \lambda_N - \epsilon) = \frac{\epsilon^{N-1}}{\prod_{i=1}^{N-1} (\lambda_N - \lambda_i)} \leq \left(\frac{\epsilon}{\lambda_N - \lambda_{N-1}} \right)^{N-1}, \quad \epsilon < \lambda_N - \lambda_{N-1}. \quad (39)$$

The upper bound goes to zero for increasing N , if

$$\lim_{N \rightarrow +\infty} N \left(1 - \frac{\epsilon}{\lambda_N - \lambda_{N-1}} \right) = +\infty, \quad (40)$$

which is likely to hold, except if the spectrum of \mathbf{Q}_α shrinks to the top (i.e., $\lambda_{N-1} \rightarrow \lambda_N$) sufficiently fast. We conjecture that this is unexpected without any symmetry in the system. It is worth noting that the exact statistics of the distributions of eigenvalues of \mathbf{Q}_α have been studied by Brouwer, Frahm and Beenakker [8], which may provide a good basis for a more in-depth treatment of this likelihood. Analogue discussions were recently performed in the case of the transmissivity distribution by Wang and Guo [37].

Further examples of collective manipulation of objects

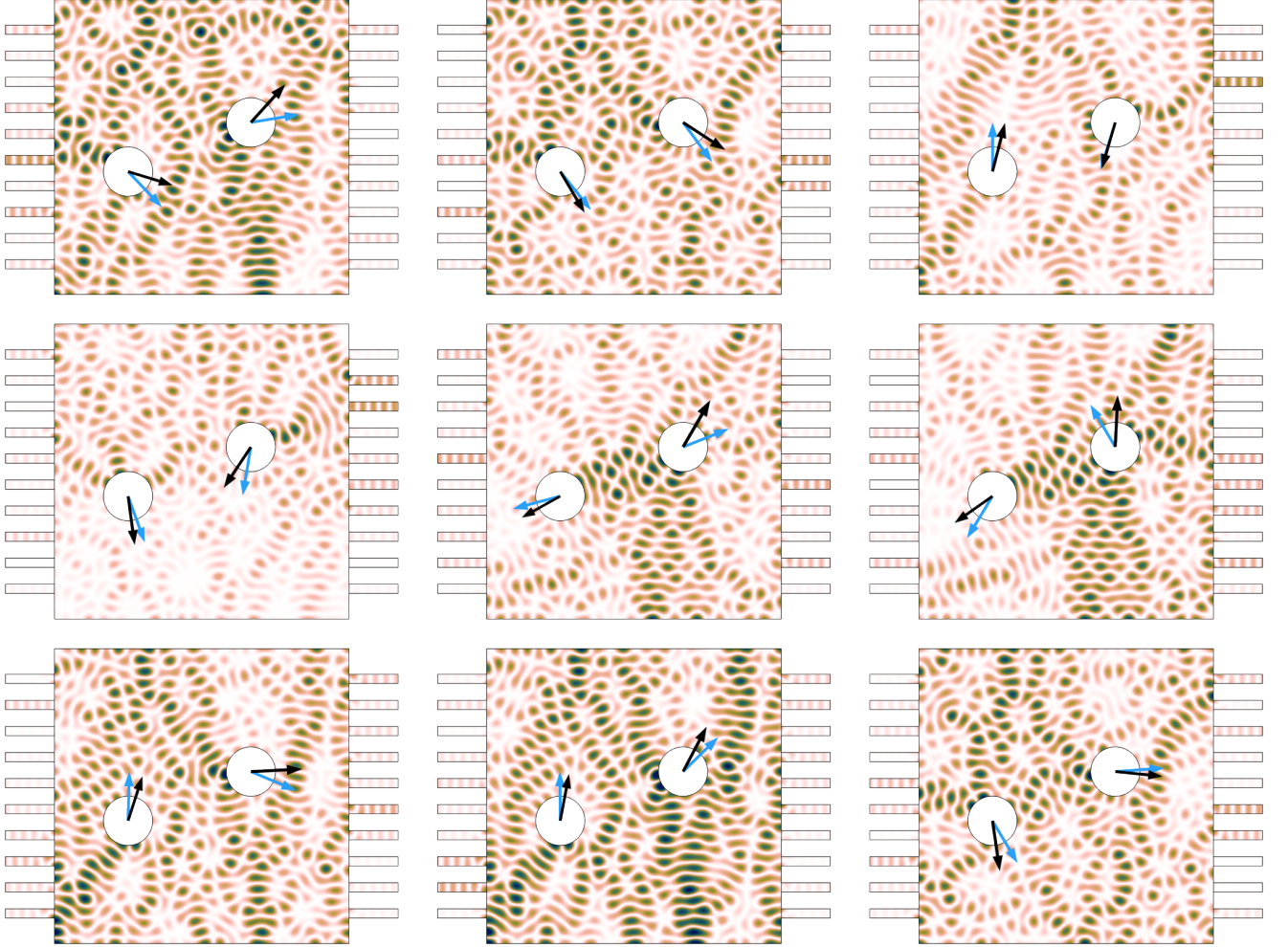


FIG. 4. Further examples of bi-objective optimization for which $\langle \mathbf{Q}_{\Delta \mathbf{r}_1} \rangle = \langle \mathbf{Q}_{\Delta \mathbf{r}_2} \rangle$. As in Fig. 2b, blue arrows represent the objectives and black arrows represent the realized Pareto-optimal net equal-projection forces on the scatterers.